The Astrophysical Journal, 834:163 (7pp), 2017 January 10 doi:10.3847/1538-4357/834/2/163

SWIFT OBSERVATIONS OF TWO OUTBURSTS FROM THE MAGNETAR 4U 0142+61

R. F. Archibald[1], V. M. Kaspi[1], P. Scholz[1,2], A. P. Beardmore[3], N. Gehrels[4], and J. A. Kennea[5]
[1] Department of Physics and McGill Space Institute, McGill University, 3600 University Street, Montreal QC, H3A 2T8, Canada; rarchiba@physics.mcgill.ca
[2] National Research Council of Canada, Herzberg Astronomy and Astrophysics, Dominion Radio Astrophysical Observatory, P.O. Box 248, Penticton, BC V2A 6J9, Canada
[3] Department of Physics and Astronomy, University of Leicester, University Road, Leicester LE1 7RH, UK
[4] Astrophysics Science Division, NASA Goddard Space Flight Center, Greenbelt, MD 20771 USA
[5] Department of Astronomy and Astrophysics, 525 Davey Lab, Pennsylvania State University, University Park, PA 16802, USA
Received 2016 October 31; revised 2016 November 29; accepted 2016 November 29; published 2017 January 11

ABSTRACT

4U 0142+61 is one of a small class of persistently bright magnetars. Here, we report on a monitoring campaign of 4U 0142+61 from 2011 July 26 to 2016 June 12 using the *Swift* X-ray Telescope, continuing a 16-year timing campaign with the *Rossi X-ray Timing Explorer*. We show that 4U 0142+61 had two radiatively loud timing events, on 2011 July 29 and 2015 February 28, both with short soft γ-ray bursts, and a long-lived flux decay associated with each case. We show that the 2015 timing event resulted in a net spin-down of the pulsar that is due to overrecovery of a glitch. We compare this timing event to previous such events in other pulsars with high magnetic fields and discuss net spin-down glitches now seen in several young, high-B pulsars.

Key words: pulsars: general – stars: magnetars – stars: neutron

1. INTRODUCTION

Magnetars are a class of young, rotating neutron stars with spin periods ranging from ~0.3 to 12 s. They appear to have the highest spin-down-inferred dipolar surface magnetic fields of the neutron-star population, with magnetic fields of order 10^{14}–10^{15} G, although magnetars with more typical inferred dipole magnetic fields have recently been found (e.g., Rea et al. 2013; Scholz et al. 2014b). Magnetars exhibit a wide array of radiative behavior, showing flux variability at nearly all timescales—from soft γ-ray bursts lasting milliseconds to X-ray increases by several orders of magnitude that decay over months to years. As implied by the name, the decay of their magnetic fields is thought to power the X-ray emission of these objects, the energy of which can be much greater than that available via the spin-down luminosity, which accounts for rotation-powered pulsar energetics (Thompson & Duncan 1995, 1996). For a recent review, see Mereghetti et al. (2015). There are currently 23 confirmed magnetars; an up-to-date list of both confirmed and candidate magnetars is maintained in the McGill Magnetar Catalog[6] (Olausen & Kaspi 2014).

Magnetars, like rotation-powered pulsars, experience sudden changes in their spin-frequency that are known as glitches (see, e.g., Kaspi et al. 2000; Dib et al. 2008). While similar in many regards to glitches in rotation-powered pulsars, magnetar glitches are unique in that they are often accompanied by radiative changes including short soft γ-ray bursts, pulse profile changes, and long-term (months to years) X-ray flux enhancements (see Rea & Esposito 2011; Dib & Kaspi 2014, for a review).

4U 0142+61 has the highest persistent X-ray flux of the known magnetars. It was discovered as a point source by the *Uhuru* mission (Giacconi et al. 1972), and was later revealed to be a ~8.7 s pulsar (Israel et al. 1994). It has an inferred dipole surface magnetic field of 1.3×10^{14} G.

[6] www.physics.mcgill.ca/~pulsar/magnetar/main.html

4U 0142+61, along with several other magnetars, was monitored regularly with the *Rossi X-ray Timing Explorer* (*RXTE*) in 1997 and from 2000 until the decommissioning of *RXTE* in 2011 December (Dib & Kaspi 2014). During this campaign, 4U 0142+61 showed a slow rise in pulsed flux accompanied by pulse profile changes from 2000 to 2006 (Dib et al. 2007). Most notably, in 2006, 4U 0142+61 entered an active phase—emitting at least six short magnetar-like bursts, and exhibiting a glitch with an overrecovery, leading to a net spin-down of the neutron star (Gavriil et al. 2011a). On 2011 July 29, 4U 0142+61 had large spin-up glitch (Dib & Kaspi 2014). This glitch was accompanied by a short hard X-ray burst detected by the *Swift* Burst Alert Telescope (BAT) (Gavriil et al. 2011b).

Compared to the other long-term *RXTE*-monitored magnetars, 4U 0142+61 is relatively quiet in terms of timing behavior. Except for the aforementioned glitches, the rotational evolution is well described by a low-order polynomial, a statement that cannot be made for any of the other sources in the *RXTE* monitoring campaign (Dib & Kaspi 2014).

Here we present the results of a continued monitoring campaign of 4U 0142+61 using the *Swift* X-ray Telescope (XRT) from 2011 July to 2016 June. We report on two X-ray outbursts on 2011 July 29 and 2015 February 28, both associated with timing anomalies. We find that the timing anomaly associated with the X-ray outburst on 2015 February 28, similar to the 2006 event, led to a net spin-down of 4U 0142+61. We also find a long-term X-ray flux decay following both timing events, as well as 12 XRT-detected magnetar-like bursts that occurred coincident with the second timing event.

2. OBSERVATIONS AND ANALYSIS

2.1. *Swift X-Ray Telescope*

We began observing 4U 0142+61 with the *Swift* XRT on 2011 July 26 as part of a campaign to monitor several magnetars (see, e.g., Scholz et al. 2014a; Archibald et al. 2015).

The *Swift* XRT (Burrows et al. 2005) is a Wolter-I telescope with a e2v CCD22 detector, sensitive in the 0.3–10 keV range. The XRT was operated in windowed-timing mode for all observations with a time resolution of 1.76 ms, at the expense of one dimension of spatial resolution.

Level 1 data products were obtained from the HEASARC *Swift* archive, reduced using the `xrtpipeline` standard reduction script, and time corrected to the solar system barycenter using the position of 4U 0142+61 (Hulleman et al. 2004), and `HEASOFT v6.17`. Individual exposure maps, spectrum, and ancillary response files were created for each orbit and then summed. When in an individual orbit the center of the source was within three pixels of a dead column or the edge of the chip, this orbit was excluded from flux and spectral fitting. We selected only Grade 0 events for spectral fitting as other event grades are more likely to be caused by background events (Burrows et al. 2005). We also removed many detected soft X-ray bursts that appear in both the source and background region, as these bursts must be instrumental in origin.

To investigate the flux and spectral evolution of 4U 0142 +61, a circle with a radius of 10 pixels centered on the source was extracted. We also used an annulus with an inner radius of 75 pixels and an outer radius of 125 pixels centered on the source to extract background events.

Swift XRT spectra were extracted from the selected regions using `extractor`, and were fit using `XSPEC` version 12.8.2.[7] Photons were grouped to ensure that each spectral bin contained one photon. As the background dominates the source below 0.7 keV, we only used photons from the 0.7–10 keV band for spectral fitting. In total, 127 XRT observations totaling 475 ks of observing time were analyzed in this work.

3. TIMING ANALYSIS

Following the processing described in Section 2.1, we derived an average pulse time-of-arrival (TOA) for each observation. To maximize the signal-to-noise ratio for obtaining TOAs for the source, photons from 0.7–10 keV were used in the timing analysis. The TOAs were obtained using a maximum likelihood (ML) method as described in Livingstone et al. (2009) and Scholz et al. (2012). The ML method compares a continuous model of the pulse profile to the photon arrival phases obtained by folding a single observation.

These TOAs were fitted to a standard pulsar timing model wherein the phase, ϕ, as a function of time, t, is described by a Taylor expansion:

$$\phi(t) = \phi_0 + \nu_0(t - t_0) + \frac{1}{2}\dot{\nu}_0(t - t_0)^2 + \frac{1}{6}\ddot{\nu}_0(t - t_0)^3 + \ldots, \quad (1)$$

where ν_0 is the rotational frequency of the pulsar at t_0, $\dot{\nu}_0$ the spin-down rate at t_0, and $\ddot{\nu}_0$ the second time derivative of the rotational frequency. This was done using the TEMPO2 (Hobbs et al. 2006) pulsar timing software package.

As we have only one *Swift* observation before the 2011 glitch on MJD 55771.19 (Dib & Kaspi 2014), we present a timing solution starting at MJD 55771.9, the first XRT observation following the aforementioned glitch. We note that the timing solution presented by Dib & Kaspi (2014) accurately describes our measured TOAs in the overlapping region.

Table 1
Phase-coherent Timing Parameters for 4U 0142+61

Dates (MJD)	55771.54-57551.22
Dates	29 July 2011–12 June 2016
Epoch (MJD)	57000.00000
ν (s^{-1})	0.115 085 312 4(3)
$\dot{\nu}$ (s^{-2})	$-2.621(2) \times 10^{-14}$
$\ddot{\nu}$ (s^{-3})	$8(3) \times 10^{-25}$
Glitch Parameters	
Glitch Epoch	57081.21605 (fixed)
$\Delta\nu$ (s^{-1})	$-3.7(1) \times 10^{-8}$
$\Delta\nu_d$ (s^{-1})	$5.1(5) \times 10^{-8}$
τ_d (days)	57(9)
rms residual (s)	0.118
rms residual (phase)	0.014

Note. Figures in parentheses are the nominal 1σ TEMPO2 uncertainties in the least-significant digits quoted.

We present a fully phase-coherent timing solution in Table 1. The basic timing solution provides an accurate description of the TOAs until MJD 57079.7. At this date, we require a change in the spin parameters to accurately describe the TOAs. We fit for a glitch with both permanent and decaying parameters wherein the spin frequency after the glitch epoch, t_g, can be described as

$$\nu(t) = \nu_t + \Delta\nu + \Delta\nu_d e^{-(t-t_g)/\tau_d}, \quad (2)$$

where ν_t is the predicted spin frequency pre-glitch, $\Delta\nu$ is a permanent change in the spin frequency, and $\Delta\nu_d$ is an exponentially decaying change in the spin frequency decaying with a timescale of τ_d days. This glitch is coincident with the 2015 February 28 BAT detection and with the short-term X-ray flux increase (see Barthelmy et al. 2015 and Section 4.2).

Owing to pulse shape variations, for the three observations immediately following the 2015 outburst –those occurring on MJDs 55782.6, 57084.1, and 57087.5, our ML TOA extraction method indicated that these three TOAs were 0.43 phase turns out of phase with all the surrounding TOAs. The profiles can be seen in Figure 1. This offset is consistent with the distance between the two peaks in the standard profile. We therefore exclude these three TOAs from our timing analysis. The full timing solution is presented in Table 1. The timing residuals, that is, the difference between the modeled and observed TOAs, can be seen in Figure 2. We note that these three suspect TOAs are in phase with each other, and that if we shift them by the time between the two profile peaks and include them in our glitch fitting procedure, they have little effect ($\sim 1\sigma$) on the reported parameters.

We emphasize that the net spin-*down* glitch properties are most affected by the TOAs long after the outburst, far away from the period of strong profile changes. To illustrate the difference in the inclusion of the suspect profiles, in Figure 2 we present the evolution of ν over the *Swift* campaign. To generate this figure, we fit splines to the pulse numbers (see Dierckx 1975) using a method similar to that described in Dib & Kaspi (2014), which uses piecewise polynomials of degree $n = 3$ weighted by the inverse square error on the pulse number. To generate the error bounds, we added Gaussian

[7] http://heasarc.gsfc.nasa.gov/docs/xanadu/xspec/index.html

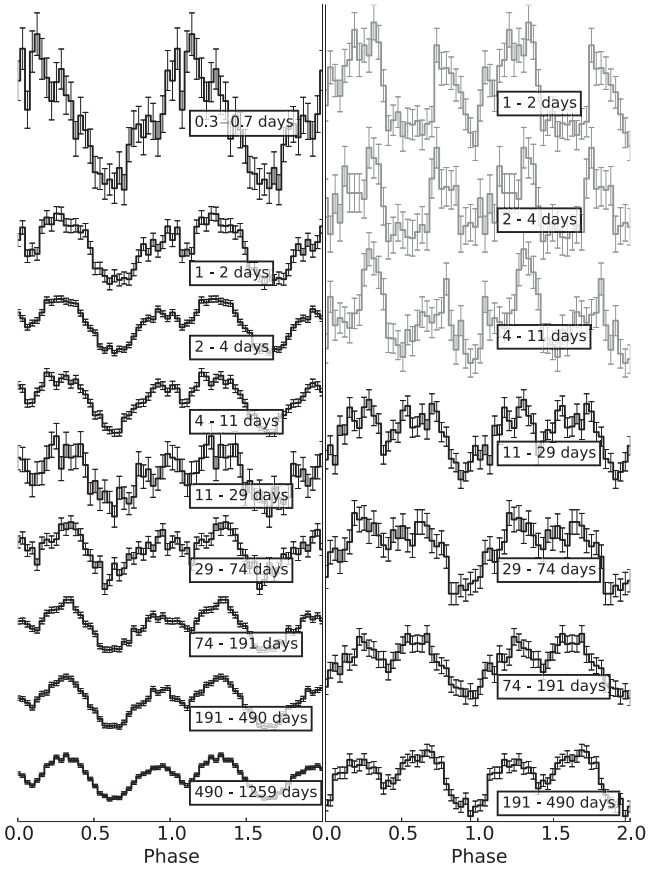

Figure 1. Pulse shape evolution of 4U 0142+61. The panels show the total 0.7–10 keV profiles, binned in equal log-time bins. The left panel present profiles following the 2011 outburst in days from MJDs 55771.19, and the right panel shows profile following the 2015 outburst in days from MJD 57081.2. The profiles have been normalized and vertically shifted to avoid overlap. The three profiles in gray are those excluded from the timing solution because of profile variations.

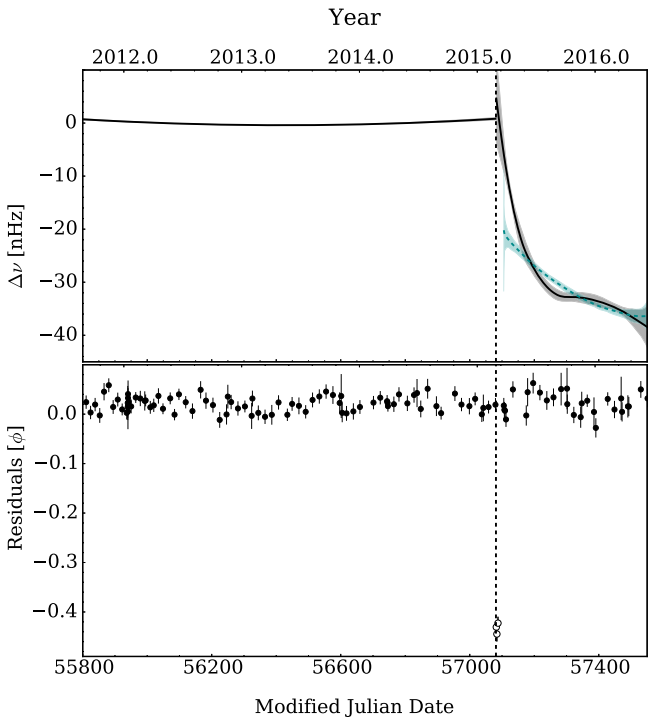

Figure 2. Timing evolution of 4U 0142+61 over the *Swift* campaign. The top panel shows ν over time with the average pre-burst $\dot{\nu}$ trend removed. The solid black line with a gray error region uses all TOAs, and the blue dashed line shows the solution excluding TOAs with strong pulse profile changes; see Section 3 for details. The bottom panel shows the timing residuals for the ephemeris presented in Table 1. The hollow points denote the TOAs excluded because of profile variations. In both panels, the dashed vertical time indicates the time of the glitch.

noise with standard deviations of the measured TOA uncertainties to these pulse numbers 1000 times, and refit the splines. The plotted error band shows the 68% confidence region. Note that while in this semicoherent solution a spin-up glitch is not required when excluding the three suspect TOAs, a fully coherent solution requires the spin-up component in either case.

4. RADIATIVE PROPERTIES

4.1. Long-term Spectral Evolution

Following the data reduction described in Section 2.1, we fit each observation using the typical phenomenological two-component model used for magnetar spectra—an absorbed blackbody plus a power law. Photoelectric absorption was modeled using `XSPEC tbabs` with abundances from Wilms et al. (2000) and photoelectric cross-sections from Verner et al. (1996).

To determine a self-consistent $N_{\rm H}$ for 4U 0142+61, we simultaneously fit observations between MJD 56260–56999, i.e., a large set of observations far away from hard X-ray burst detections, and where the flux and spectral parameters of the individual observations were consistent. We fit these to a single absorbed blackbody plus power law and obtained $N_{\rm H} = (1.11 \pm 0.04) \times 10^{22}\,{\rm cm}^{-2}$ at 90% confidence with a C-statistic (Cash 1979) of 18779.89 for 18553 degrees of freedom. For all other spectral results presented here, we therefore assumed a constant value of $N_{\rm H} = 1.11 \times 10^{22}\,{\rm cm}^{-2}$.

In Figure 3 we show the absorbed 0.5–10 keV flux, the power-law index, Γ, and the blackbody temperature, kT, for each observation. We note that these two parameters are highly covariant because of their similar contributions to the flux in this band, and we urge caution in interpreting any apparent trend. The epochs where 4U 0142+61 triggered the *Swift* BAT are indicated in the plot with vertical black lines: the dotted black line indicates the BAT trigger without a corresponding glitch, and the dashed lines indicate triggers assocated with glitches. Moreover, the black arrow in the plot indicates that on MJD 57081.2 the flux was several times higher than the persistent level, decaying within a single orbit, and it contained several magnetar-like bursts. See Section 4.2 for further details.

Taken with the marginal pulsed flux increase seen with *RXTE* (Dib & Kaspi 2014), we can confirm using the XRT data that the 2011 glitch was a radiatively loud event. To characterize this radiative behavior, we tried fitting the inter-glitch flux decay between MJDs 55771 and 57079 with a power law, a linear decay, and an exponential decay, all plus a quiescent flux. As none of these single-component models provided a statistically acceptable fit, we then fitted models with either two power-law decays ($\chi^2/{\rm dof} = 90.8/70$) or two exponentials, both plus a constant quiescent flux. The best fitting of these models, with $\chi^2/{\rm dof} = 48.0/70$, is the double exponential, as described by the following equation: $F(t) = F_Q + F_1 e^{-(t-t_0)/\tau_1} + F_2 e^{-(t-t_0)/\tau_2}$, where F_Q is the "quiescent" flux, fixed at $12.4(4) \times 10^{-11}\,{\rm erg\,s^{-1}\,cm^{-2}}$, the level measured on MJD 55768.7, the date of the last XRT

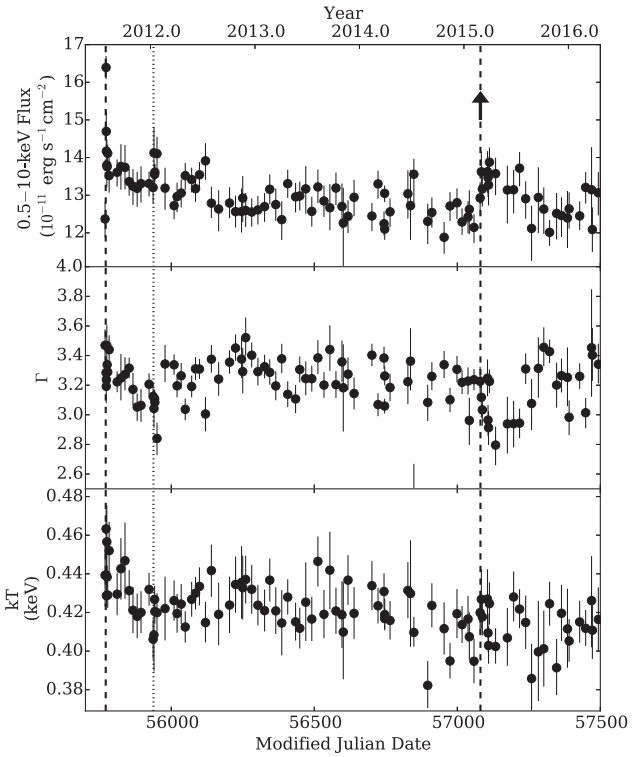

Figure 3. Flux and spectral evolution of 4U 0142+61 during *Swift* monitoring. The top panel shows the absorbed 0.5–10 keV flux. The vertical dashed lines indicate *Swift* BAT triggers associated with glitches, and the vertical dotted line indicates the BAT trigger with no associated timing behavior. The black arrow indicates the point at which the flux increases by a factor of 10 and decays on timescales of minutes (see Section 4.2 and Figure 5). The central panel shows Γ, the power-law index, and the bottom panel shows *kT*, the blackbody temperature, as a function of time.

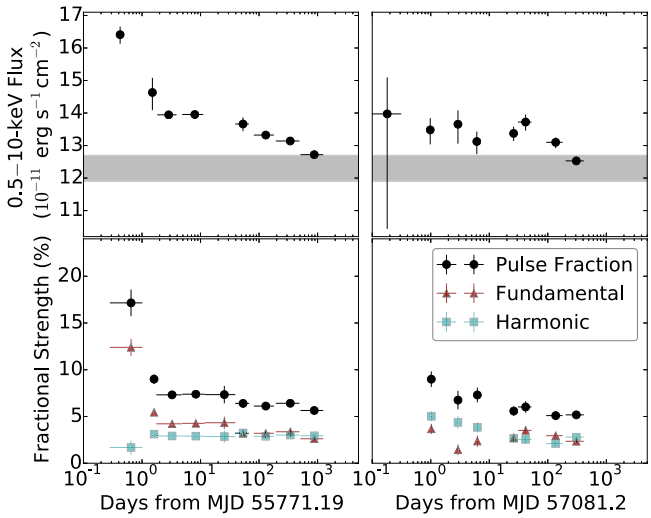

Figure 4. Flux and pulse shape evolution of 4U 0142+61. The top panels show the total absorbed 0.5–10 keV flux, binned in equal log-time bins from MJDs 55771.19 and 57081.2. The gray band in the upper panels shows the pre-2011 outburst flux value. The lower panels show the 0.7–10 keV rms pulsed fraction as black circles, the strength in the fundamental (i.e., at the spin frequency) as red triangles, and first harmonic (i.e., at twice the spin frequency) as blue squares, with the same time binning.

observation prior to the flux increase. The best-fit parameters are $F_1 = 13(7) \times 10^{-11}$ erg s^{-1} cm^{-2}, $\tau_1 = 0.6(2)$ days, $F_2 = 1.4(1) \times 10^{-11}$ erg s^{-1} cm^{-2}, and $\tau_2 = 510(80)$ days. Note that all values here are absorbed 0.5–10 keV fluxes, and t_0 is held fixed at the time of the *RXTE* reported glitch, MJD 55771.19.

We also fitted the long-term decay in X-ray flux following the 2015 glitch. In this case, we required only a single exponential decay, again fixing the quiescent flux at $12.4(4) \times 10^{-11}$ erg s^{-1} cm^{-2}. The best-fit parameters give a flux increase of $F = 1.3(3) \times 10^{-11}$ erg s^{-1} cm^{-2} with a decay time of $\tau = 160(70)$ days with χ^2/dof = 13.7/21. The flux decay can be more clearly seen in Figure 4, where the data have been binned.

The X-ray pulse profile of 4U 0142+61 has been shown to evolve over a timescale of years (Dib et al. 2007). We therefore investigated the evolution of the pulse profile at the timescales suggested by the decaying total flux. To do so, we folded all aforementioned XRT observations into 32-bin profiles using the timing solution presented in Table 1, and created a profile for each equally logarithmically spaced segment of the time series following each of the two timing events. We then transformed these profiles into their respective Fourier representations, allowing us to quantify both the pulse shape and root mean squared (rms) pulsed fraction. For details on the rms pulsed fraction, see, e.g., An et al. (2015). In Figure 4 we present the pulsed fraction and power in the first two Fourier harmonics over time. For reference, in the top panel we show the total absorbed 0.5–10 keV flux binned at the same time resolution. The pulse profiles themselves can be seen in Figure 1. It is clear that the pulsed fraction of the source decreased rapidly starting from the 2011 glitch, mirroring the behavior of the total X-ray flux. This was driven primarily by a decrease in the strength of the fundamental. Following both glitches the pulse profile shows variability for approximately 10 days following the glitch before reattaining the normal state with both the fundamental and harmonic having equal power, as can be seen in Figure 4.

4.2. Short-term Flux Enhancement and Bursts

Immediately following the BAT trigger on MJD 57081, 2015 Febuary 28 (Barthelmy et al. 2015), the XRT slewed to observe 4U 0142+61. For the first snapshot of observation, the source was significantly brighter and harder than in the surrounding observations. Fitting an absorbed blackbody plus power law was not warranted, as the spectrum is well fit (C-stat of 904 for 947 degrees of freedom) by an absorbed power law with $\Gamma = 1.68(5)$ and an absorbed 0.5–10 keV flux of $1.06(3) \times 10^{-9}$ erg s^{-1} cm^{-2}. However, we note that this is an average flux for this snapshot. The flux evolved on a faster timescale than this, and a more complicated short-term flux evolution is clear. This is evident in the binned light curve of the XRT snapshot taken after the BAT trigger, shown in Figure 5 with a reference line plotted at the average count rate for 4U 0142+61.

We searched all *Swift* XRT observations for magnetar-like bursts at timescales of 1, 0.1, and 0.01 s. This was done following the method of Scholz & Kaspi (2011), wherein for each Good Time Interval, statistically significant deviations from the mean count rate are flagged, assuming Poisson statistics. Because of the aforementioned instrumental bursts, the burst search was run only on photons having energies greater than 0.7 keV. We detected significant bursts only in the XRT data in the observations following the 2015 February 28 BAT detection (Barthelmy et al. 2015). Eleven bursts were found in this observation, superimposed on an overall flux decrease with a decay rate on the order of 100 s.

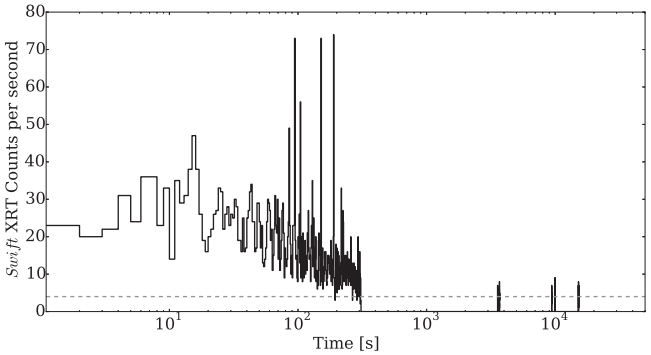

Figure 5. *Swift* XRT light curve in the 0.7–10 keV band for the 2015 Febuary 28 burst observation. The light curve has been binned at 1 s. The gray dashed line represents the average count rate of 4U 0142+61.

In addition, one burst was detected in the observation one day later. In Table 2 we present the burst times in seconds from MJD 57081.2043746, the total fluences, T_{90} (the time period that contains 90% of a bursts fluence), and the phase at which the peak of the burst occurred. The properties of these bursts are typical for magnetars (Collazzi et al. 2015).

We also note a third BAT detection of 4U 0142+61 on 2012 January 12 (Barthelmy et al. 2012). This burst was unaccompanied by any timing event or long-term radiative change. While this lack of associated timing event is unique among the three BAT detections presented here, this is not an atypical behavior for magnetars. For example, 1E 1841−045 has triggered BAT on several occasions with no measurable change in its timing properties (An et al. 2015).

5. DISCUSSION

In this work, we have presented the evolution of the pulse profile, flux, and timing parameters of 4U 0142+61 from July 2011 to June 2016. Over this monitoring campaign, we report two timing events, both accompanied by changes in the radiative behavior of the magnetar, as well as a BAT-detected burst with no other associated behavior.

The first timing event occurred in 2011 and was characterized by a simple step-like glitch in spin frequency heralded by a BAT-detected bright X-ray burst. This glitch was followed by an X-ray flux decay with two timescales—an initial fast decay with $\tau = 0.6(2)$ days and a longer $\tau = 510(80)$ day decay.

The second timing event in the *Swift* campaign occurred in 2015. This glitch had a more complex timing structure that required a two-component model with a 57(9) day timescale, resulting in a net spin down of the pulsar, see Table 1. This event was also accompanied by a BAT-detected bright X-ray burst, as well as a long-lived flux decay with $\tau = 160(70)$ days. This second event bears a striking resemblance to the 2006 outburst from this same source (Gavriil et al. 2011a). Both began with a ∼100 s timescale X-ray flux increase, accompanied by several clustered magnetar-like short X-ray bursts and a timing event resulting in a net spin-down of the pulsar. The long-term X-ray flux evolution of 4U 0142+61 is quite typical for a magnetar: the spectrum becomes harder at the time of the outburst; see Section 4.2.

Table 2
Swift XRT-detected Burst Parameters from 4U 0142+61 during the 2015 February Event

Burst time s from start	T_{90} ms	Fluence 1–10 keV Photons	Phase ϕ(0–1)
37.46	103 ± 5	14 ± 4	0.48
66.48	39 ± 14	12 ± 3	0.82
85.60	110 ± 80	19 ± 4	0.02
94.80	450 ± 60	61 ± 8	0.08
104.16	170 ± 50	37 ± 6	0.16
151.81	260 ± 20	56 ± 7	0.64
189.28	110 ± 30	48 ± 7	0.95
217.46	80 ± 50	22 ± 5	0.19
225.50	400 ± 300	17 ± 4	0.12
256.97	500 ± 100	19 ± 4	0.74
301.77	400 ± 300	7 ± 3	0.90
85,866.90	30 ± 20	7 ± 3	0.17

5.1. Radiative Evolution

There are two main classes of models to explain the flux evolution of magnetar outbursts: neutron star cooling and magnetospheric relaxation. Both sets of models can explain the differing timescales for outbursts from the same source, a common feature in magnetar outbursts (e.g., Gavriil & Kaspi 2004; Bernardini et al. 2011; An et al. 2012).

In neutron star cooling models, the long-term flux evolution following a magnetar outburst is a thermal relaxation of the crust of the neutron star until it reattains thermal equilibrium with the core. In this model, the differing timescales for different events in the same source may be related to energy being injected at different depths into the crust of the neutron star (Brown & Cumming 2009; Scholz et al. 2012; Deibel et al. 2015), with longer timescales corresponding to deeper layers in the crust.

The other major class of models that describes the flux relaxation of magnetars following outbursts involves the untwisting of the magnetosphere (e.g., Beloborodov 2009). In this model, current carrying field lines, *j*-bundles, have been twisted by crustal motion following the outbursts. These twists are anchored to the surface and bombard the surface with accelerated charged particles, heating the surface. As the twist dissipates, the area affected by the bombardment shrinks and cools. This has an expected decay time of $t_{ev} \sim 10^7\ \mu_{32}\ \Phi_{10}^{-1}\ A_{11.5}$ s, where μ_{32} is the magnetic moment in units of 10^{32} G cm^3, Φ_{10} is the electric voltage sustaining electron-positron discharge in the magnetosphere in units of 10^{10} V, and $A_{11.5}$ is the area of the *j*-bundle footprint in units of $10^{11.5}$ cm^2. With the parameters of 4U 0142+61, this timescale should be $t_{ev} \sim 10^7\Phi_{10}^{-1}$ s $\sim 150\Phi_{10}^{-1}$ days, roughly consistent with the flux decay timescale of the 2015 outburst. In this model, these different timescales would be due to different values of Φ_{10}, as the magnetic moment of the neutron star has not changed, and the blackbody area has only changed at the ∼10% level over this campaign.

5.2. Glitches in High-B pulsars

Glitches in pulsars often result in both a permanent step in spin frequency and components that decay—typically with the functional form of an exponential. In standard pulsar glitch theory, glitches and their recoveries are an observable of the

Table 3
Reported Net Spin-down Glitches

Pulsar	B-field 10^{14} G	Long-term $\Delta\nu$ Hz	Timescale Days	Q	Radiative Behavior	Reference
SGR 1900+14	7.0	$-1.10(3) \times 10^{-4}$	<80	⋯	giant flare, bursts	Woods et al. (1999)
PSR J1846–0258	0.49	$-9.52(9) \times 10^{-5}$	127(5)	8.7(2.5)	bursts, flux increase	Livingstone et al. (2010)[a]
1E 2259+586	0.59	$-4.5(6) \times 10^{-8}$	<4	⋯	burst, flux increase	Archibald et al. (2013)[b]
1E 2259+586	0.59	$-1.2(3) \times 10^{-8}$	⋯	⋯	flux increase	Içdem et al. (2012), Dib & Kaspi (2014)
4U 0142+61	1.3	$-1.27(17) \times 10^{-8}$	17(1.7)	1.07(2)	bursts, flux increase	Gavriil et al. (2011a)[c]
4U 0142+61	1.3	$-3.7(1) \times 10^{-8}$	57(9)	3.6(4)	bursts, flux increase	This work[d]
1E 1841–045[e]	7.0	$-4.9(6) \times 10^{-8}$	⋯	⋯	⋯	Şaşmaz Muş et al. (2014)[f]

Notes.
[a] Accompanied by decaying spin-up glitch with $\Delta\nu = 10.8(4) \times 10^{-5}$ Hz.
[b] Possibly accompanied by second glitch event.
[c] Accompanied by decaying spin-up glitch with $\Delta\nu = 2.0(4) \times 10^{-7}$ Hz.
[d] Accompanied by decaying spin-up glitch with $\Delta\nu = 5.1(5) \times 10^{-8}$ Hz.
[e] Disputed events, see the notes below.
[f] Not seen in analysis of same data by Dib & Kaspi (2014).

coupling between the neutron superfluid and non-superfluid components of the crust (e.g., Anderson & Itoh 1975). For typical glitches that result in a spin-up of the neutron star, the sudden spin-up is explained as a transfer of angular momentum from the superfluid component to the solid components of the crust. This will result in a spin-up of the neutron star as the superfluidic component has more angular momentum than the crust because the crust suffers external spin-down torque. When the superfluid and solid components become coupled, the superfluid will have a higher angular velocity and transfer some of this extra angular momentum to the solid crust. For a more thorough review of pulsar glitch theory, see Haskell & Melatos (2015).

In this standard picture, spin-down glitches can occur via the transfer of angular momentum from the inner crust, which may have slower spinning regions due to plastic crustal deformation caused by the extreme magnetic field (e.g., Thompson et al. 2000). The long-term X-ray pulse profile and pulsed fraction evolution, such as that presented in Section 4.1, could be evidence for the slow, plastic deformation of the crust needed to produce slower regions of superfluid (Woods et al. 2004; Thompson et al. 2002).

Alternatively, regions of the outer core could be involved as a result of the strong magnetic fields. Magnetar strength fields provide a strong pinning of vortices to flux tubes in the outer core, which leads to a rotation lag between the normal and superfluid components, which, when relaxed, would lead to a spin-down event (Kantor & Gusakov 2014).

In typical rotation-powered pulsars, the expected internal nature of these spin-up glitches is argued to be indicated by the lack of observed radiative changes. This "radiatively quiet" condition does not hold for many glitches in magnetars. Many magnetar glitches are accompanied by drastic changes in their X-ray flux and pulse profiles (e.g., Kaspi et al. 2003; Dib et al. 2009). This could indicate that external forces are at play in radiatively loud glitches, and these external forces may lead to the net spin-down events reported in several magnetars, including the new event reported here.

We have compiled a list of all published confirmed and candidate net spin-down glitches in Table 3. In this list, we present the magnitude of the change in spin frequency, $\Delta\nu$. For net spin-down glitches that are due to overrecovering spin-up glitches, the τ_d of the glitch is presented. For events where there is no sign of a recovery, we show an upper limit for the time during which the spin-down had to occur. We also note that 6 of the 7 reported net spin-down glitches are accompanied by radiative changes.[8] This is a much higher fraction of radiative activity than seen in spin-up events, where only 5 of 22 timing anomalies were accompanied by radiative changes (Dib & Kaspi 2014).

For the net spin-down glitches in which the net spin down is measured to be due to an overrecovery, we also report the recovery fraction, Q. Recovering glitches are often classified by their recovery fraction, defined as $Q \equiv \Delta\nu_d/(\Delta\nu_d + \Delta\nu)$. In younger pulsars, when recoveries are observed, Q tends to be larger than in older pulsars (Wang et al. 2000). For the new glitch we report here, we measure $Q = 3.6 \pm 0.4$. Glitches with $Q > 1$ have only been seen twice before: once following the magnetar-like outburst of the pulsar PSR J1846−0258 that is powered by a high magnetic field rotation, which had $Q = 8.7 \pm 2.5$ (Livingstone et al. 2010), and once during the 2006 outburst of 4U 0142+61 with $Q = 1.07 \pm 0.02$ (Gavriil et al. 2011a). Interestingly, all three of these overrecovering glitches were accompanied by radiative behavior. Indeed, it should be noted that as a result of the necessary non-continuous monitoring strategies used to study magnetars, all of the net spin-down events, i.e., the "anti-glitches," may be unresolved overrecovering glitches, albeit with a short timescale. The most constraining limit placed on an unresolved overrecovery timescale is shorter than four days in the 2012 glitch of the magnetar 1E 2259+586. (Archibald et al. 2013).

The radiatively loud nature of these spin-down glitches could be symptomatic of external changes, e.g., the magnetosphere (Beloborodov 2009; Parfrey et al. 2012, 2013). However, magnetars also exhibit typical spin-up glitches that are accompanied by similar radiative changes (e.g., Kaspi et al. 2003; Dib et al. 2009), which could indicate that another variable is at play. One possibility for this is the location of the twist in the magnetosphere. The observed radiative properties of magnetars are determined by their closed field, whereas the spin-down properties are dominated by the open field lines (e.g., Beloborodov & Thompson 2007; Beloborodov 2009). Therefore, whether or not the closed field line region is affected

[8] This increases to 6 of 6 if we ignore the disputed event; see Table 3.

during a twist event could determine if a glitch is accompanied by a radiative outburst.

6. CONCLUSION

We have presented the results of a 5-year monitoring campaign of 4U 0142+61 using the *Swift* XRT. Over this campaign, we have shown that 4U 0142+61 has had two X-ray outbursts associated with timing events, one in 2011, and a second in 2015. The 2011 outburst was accompanied by a simple step-like spin-up glitch in spin frequency (Dib & Kaspi 2014). The 2015 outburst was accompanied by an unusual glitch, starting with a spin-up in the spin frequency that decayed with a 57(9)-day timescale, resulting in a net spin-down of the pulsar.

As the sample of timing anomalies in magnetars continues to grow, we are detecting more net spin-down events that have not been detected in the normal radio pulsar population. This strongly implicates the influence of a large magnetic field in spin-down events and, coupled with the radiatively loud nature of the plurality of spin-down events, suggests an origin in the magnetosphere of the star.

We are grateful to the *Swift* team for their flexibility in the scheduling of the timing monitoring campaign of 4U 0142 +61. We thank A. Cumming for helpful discussions. R.F.A. acknowledges support from an NSERC Alexander Graham Bell Canada Graduate Scholarship. V.M.K. receives support from an NSERC Discovery Grant and Accelerator Supplement, Centre de Recherche en Astrophysique du Quebec, an R. Howard Webster Foundation Fellowship from the Canadian Institute for Advanced Study, the Canada Research Chairs Program and the Lorne Trottier Chair in Astrophysics and Cosmology. P.S. acknowledges support from a Schulich Graduate Fellowship from McGill University. We acknowledge the use of public data from the *Swift* data archive. This research has made use of data obtained through the High Energy Astrophysics Science Archive Research Center Online Service, provided by the NASA/Goddard Space Flight Center.

REFERENCES

An, H., Archibald, R. F., Hascoët, R., et al. 2015, ApJ, 807, 93
An, H., Kaspi, V. M., Tomsick, J. A., et al. 2012, ApJ, 757, 68
Anderson, P. W., & Itoh, N. 1975, Natur, 256, 25
Archibald, R. F., Kaspi, V. M., Ng, C.-Y., et al. 2013, Natur, 497, 591
Archibald, R. F., Kaspi, V. M., Ng, C.-Y., et al. 2015, ApJ, 800, 33
Barthelmy, S. D., D'Elia, V., Gehrels, N., et al. 2012, GCN, 12829, #1
Barthelmy, S. D., Gehrels, N., Kennea, J. A., et al. 2015, GCN, 17507, 1
Beloborodov, A. M. 2009, ApJ, 703, 1044
Beloborodov, A. M., & Thompson, C. 2007, ApJ, 657, 967
Bernardini, F., Israel, G. L., Stella, L., et al. 2011, A&A, 529, A19
Brown, E. F., & Cumming, A. 2009, ApJ, 698, 1020
Burrows, D. N., Hill, J. E., Nousek, J. A., et al. 2005, SSRv, 120, 165
Şaşmaz Muş, S., Aydın, B., & Göğüş, E. 2014, MNRAS, 440, 2916
Camilo, F., Ransom, S. M., Halpern, J. P., et al. 2016, ApJ, 820, 110
Cash, W. 1979, ApJ, 228, 939
Collazzi, A. C., Kouveliotou, C., van der Horst, A. J., et al. 2015, ApJS, 218, 11
Deibel, A., Cumming, A., Brown, E. F., & Page, D. 2015, ApJL, 809, L31
Dib, R., & Kaspi, V. M. 2014, ApJ, 784, 37
Dib, R., Kaspi, V. M., & Gavriil, F. P. 2007, ApJ, 666, 1152
Dib, R., Kaspi, V. M., & Gavriil, F. P. 2008, ApJ, 673, 1044
Dib, R., Kaspi, V. M., & Gavriil, F. P. 2009, ApJ, 702, 614
Dierckx, P. 1975, JCoAM, 1, 165
Gavriil, F. P., Dib, R., & Kaspi, V. M. 2011a, ApJ, 736, 138
Gavriil, F. P., & Kaspi, V. M. 2004, ApJL, 609, L67
Gavriil, F. P., Kaspi, V. M., Livingstone, M. A., Scholz, P., & Archibald, R. 2011b, ATel, 3520, 1
Giacconi, R., Murray, S., Gursky, H., et al. 1972, ApJ, 178, 281
Haskell, B., & Melatos, A. 2015, IJMPD, 24, 1530008
Hobbs, G. B., Edwards, R. T., & Manchester, R. N. 2006, MNRAS, 369, 655
Hulleman, F., van Kerkwijk, M. H., & Kulkarni, S. R. 2004, A&A, 416, 1037
Içdem, B., Baykal, A., & Inam, S. Ç. 2012, MNRAS, 419, 3109
Israel, G. L., Mereghetti, S., & Stella, L. 1994, ApJL, 433, L25
Kantor, E. M., & Gusakov, M. E. 2014, ApJL, 797, L4
Kaspi, V. M., Gavriil, F. P., Woods, P. M., et al. 2003, ApJL, 588, L93
Kaspi, V. M., Lackey, J. R., & Chakrabarty, D. 2000, ApJL, 537, L31
Livingstone, M. A., Kaspi, V. M., & Gavriil, F. P. 2010, ApJ, 710, 1710
Livingstone, M. A., Ransom, S. M., Camilo, F., et al. 2009, ApJ, 706, 1163
Mereghetti, S., Pons, J. A., & Melatos, A. 2015, SSRv, 191, 315
Olausen, S. A., & Kaspi, V. M. 2014, ApJS, 212, 6
Parfrey, K., Beloborodov, A. M., & Hui, L. 2012, ApJL, 754, L12
Parfrey, K., Beloborodov, A. M., & Hui, L. 2013, ApJ, 774, 92
Pintore, F., Bernardini, F., Mereghetti, S., et al. 2016, MNRAS, 458, 2088
Rea, N., & Esposito, P. 2011, ASSP, 21, 247
Rea, N., Israel, G. L., Pons, J. A., et al. 2013, ApJ, 770, 65
Scholz, P., Archibald, R. F., Kaspi, V. M., et al. 2014a, ApJ, 783, 99
Scholz, P., & Kaspi, V. M. 2011, ApJ, 739, 94
Scholz, P., Kaspi, V. M., & Cumming, A. 2014b, ApJ, 786, 62
Scholz, P., Ng, C.-Y., Livingstone, M. A., et al. 2012, ApJ, 761, 66
Thompson, C., & Duncan, R. C. 1995, MNRAS, 275, 255
Thompson, C., & Duncan, R. C. 1996, ApJ, 473, 322
Thompson, C., Duncan, R. C., Woods, P. M., et al. 2000, ApJ, 543, 340
Thompson, C., Lyutikov, M., & Kulkarni, S. R. 2002, ApJ, 574, 332
Verner, D. A., Ferland, G. J., Korista, K. T., & Yakovlev, D. G. 1996, ApJ, 465, 487
Wang, N., Manchester, R. N., Pace, R. T., et al. 2000, MNRAS, 317, 843
Wilms, J., Allen, A., & McCray, R. 2000, ApJ, 542, 914
Woods, P. M., Kaspi, V. M., Thompson, C., et al. 2004, ApJ, 605, 378
Woods, P. M., Kouveliotou, C., van Paradijs, J., et al. 1999, ApJL, 524, L55